3D SADDLE POINT DETECTION AND APPLICATIONS IN CARDIAC IMAGING

A. Fuster[⋆] *R.F.P. van Pelt*[†] *R.H.J. Fick*[†] *G. Claassen*[†] *B.M. ter Haar Romeny*[†]
H.C. van Assen[†] *L.M.J. Florack*[⋆†]

[⋆] Department of Mathematics and Computer Science
[†] Department of Biomedical Engineering
Eindhoven University of Technology, Eindhoven, The Netherlands

ABSTRACT

We investigate saddle points in 3D cardiac images. We do so by improving a critical point detection algorithm, the 3D winding number, or Poincaré index. We consider two different applications. We estimate cardiac motion from 3D tagged MRI data, based on tracking of saddle points. We also employ our method for saddle point extraction in blood flow data, acquired by phase contrast MRI.

Index Terms— tagged MRI, phase contrast MRI, saddle points, winding number, Poincaré index.

1. INTRODUCTION

Critical points are powerful features for many applications in computer vision, such as segmentation, image matching, interpolation and motion estimation [1, 2, 3, 4]. Critical point detection methods have been extensively employed for two-dimensional applications [5, 6, 7]. However, the advent of 3D acquisition technology in medical imaging calls for efficient and effective 3D critical point techniques. In this paper we address the detection of a particular type of critical points, namely 3D saddle points, and show two different applications in cardiac imaging. These concern cardiac motion estimation and characterization of blood flow dynamics. Cardiac disease may strongly influence the dynamic behaviour of the cardiac muscle. Blood flow dynamics is affected in the case of pathologic cardiovascular morphology, such as stenoses or aneurysms.

Estimation of cardiac motion is a key element for disease diagnosis and prognosis. However, there are few motion estimation algorithms available for 3D cardiac images [8, 9, 10]. Recently a promising algorithm was presented, based on the velocity over time of detected maxima in tagged MRI images [4]. Here, we investigate cardiac motion by tracking 3D saddle points instead, with the goal of achieving a more dense velocity field. This would reduce spurious effects of interpolation and thus account for a more realistic motion field. Subsequently we consider blood flow data acquired by phase contrast MRI (PC-MRI), and investigate the presence of saddle points. Blood flow plays an important role in the progression of cardiovascular diseases. It is therefore desirable to understand its complex dynamical behavior. One way to investigate velocity fields, such as blood flow data, is to investigate their topological structure. Critical points are of particular interest (see, e.g., [11]). The only genuine critical points present in the blood flow field are saddle points, given that blood flow is a closed system. In particular, saddle points are expected where flow regions with different behaviour meet [12]. However, extracting critical points of measured flow data is impaired by noise and partial volume effects.

The paper is organized as follows. We first introduce briefly the method used to extract critical points, namely, the 3D winding number algorithm [13]. This method provides information on both location and character of critical points, and it is robust with respect to noise [14]. In principle, this algorithm can detect not only extrema but also saddle points. However, no experimental results concerning saddle points were presented by Becciu et al. [13]. We show novel results on saddle point detection by the 3D winding number algorithm, both for 3D tagged MRI cardiac data and PC-MRI blood flow data. Moreover, we have optimized the algorithm and adapted it for use on flow data. Finally we discuss our results and possibilities for future work.

2. METHOD

In the case of a scalar image $u(\mathbf{x})$, critical points are those for which $\nabla u(\mathbf{x}) = 0$. In any other case the point is called regular. In 3D, there are four types of non-degenerate critical points, i.e., the determinant of the 3×3 Hessian matrix is non-zero. These are minima, 1-saddles, 2-saddles and maxima. They are commonly characterized by the number of negative eigenvalues of the Hessian, the so-called index, which is 0, 1, 2 or 3, respectively.

In order to detect saddle points, we compute the 3D winding number ν at every point in the image. We follow hereby

the definition of Kalitzin et al. [14]:

$$\nu = \oint_S \Phi(\mathbf{x}) \tag{1}$$

where Φ is a 2-form given by:

$$\Phi = \frac{u_i \, du_j \wedge du_k \epsilon^{ijk}}{(u_l u_l)^{3/2}}, \quad i,j,k,l = x,y,z \tag{2}$$

and S is a sufficiently small closed surface surrounding the point $\mathbf{x}$. Here, $u = u(\mathbf{x})$ is the image function, u_x, u_y, u_z are the components of the spatial gradient of the intensity function, $\nabla u = (u_x, u_y, u_z)$, and ϵ is the Levi-Civita symbol, defined in Cartesian coordinates as the completely antisymmetric symbol normalized by $\epsilon_{123} = 1$. The antisymmetric wedge product is represented by $\wedge$. We use Einstein's summation convention, i.e., repeated upper and lower indices are tacitly summed over. Eq. (2) can be rewritten as [13]:

$$\Phi = \frac{1}{\|\nabla u\|^3} \, [(\nabla u_i \times \nabla u_j) \cdot \nabla u] \, dx^i \wedge dx^j, \quad i,j = x,y,z \tag{3}$$

where $\nabla u_i = (u_{xi}, u_{yi}, u_{zi})$. The 3D winding number ν, given by Eqs. (1) and (3), is zero at a regular point, and $4k\pi$, with $k = \pm 1$, at a critical point [15]. The value of k depends on the character of the critical point, namely, $k = +1$ for minima and 2-saddles, and $k = -1$ for maxima and 1-saddles. Once the winding number has been calculated, it suffices to examine the image intensity at the considered point and its close neighborhood to distinguish between a minimum and a 2-saddle, or a maximum and a 1-saddle. A more detailed discussion on the derivation and properties of ν can be found in [13, 14].

In order to implement expression (3) we employ a scale-space approach [16, 17], and consider Gaussian derivatives of the image intensity function at different scales. We optimize two aspects of the winding number algorithm with respect to previous work [13]. On the one hand, we decrease computational time by exploiting the separability of the Gaussian kernel for the calculation of first and second order 3D derivatives in Eq. (3). On the other hand, we filter detected clusters of points to find the voxel with the lowest gradient magnitude, since the algorithm typically detects a cluster of critical point candidates around the true critical point. The 3D velocity field $\vec{V} = (V^1, V^2, V^3)$ of detected critical points in a sequence of frames can be computed by [4, 13]:

$$\vec{V}(t) = -H(\mathbf{x}(t), t)^{-1} \frac{\partial(\nabla u(\mathbf{x}(t), t))}{\partial t} \tag{4}$$

where t represents the different frames in the image sequence and H is the Hessian matrix.

The winding number method can also be used to find critical points of a vector field $\vec{v}(\mathbf{x})$, i.e., isolated zeros of the field. In order to do so, the algorithm has to be modified by considering the vector field $\vec{v}(\mathbf{x})$ as input data rather than the derived gradient field $\nabla u(\mathbf{x})$. We now rewrite Eq. (3) accordingly:

$$\Phi = \frac{1}{\|\vec{v}\|^3} \, [(\vec{v}_i \times \vec{v}_j) \cdot \vec{v}] \, dx^i \wedge dx^j \quad i,j = x,y,z \tag{5}$$

where $\vec{v} = (v^1, v^2, v^3)$ and $\vec{v}_i = \partial_i \vec{v} = (v_i^1, v_i^2, v_i^3)$. Subsequently, critical point detection proceeds as in the scalar case. Note that this is essentially the same critical point detection method as the so-called Poincaré index [18, 19, 20]. This nomenclature appears in, e.g., literature on flow topology and visualization, while the winding number is commonly used in the context of image analysis. Also, critical points of a vector field are referred to as source (minimum), repelling saddle (1-saddle), attracting saddle (2-saddle) and sink (maximum).

3. EXPERIMENTAL RESULTS

3.1. Cardiac motion estimation

We consider tagged MRI data of a human hart [21]. The data is a sequence of 23 volume images with a spatial resolution of $112 \times 112 \times 112$ voxels, a temporal resolution of 30 ms and tags of 8 voxels wide. We employ the described method to detect critical points in several frames of the tagged MRI data. Results depend on the scale at which derivatives are computed. This is illustrated in Fig. 1. Note that the number of saddle points is significantly higher than that of extrema. Subsequently, we compute the velocity field using Eq. (4), based on the detected saddle points and maxima. Results are given in Fig. 2. It is clear that velocity fields corresponding to both types of saddle points are substantially more dense than in the case of maxima.

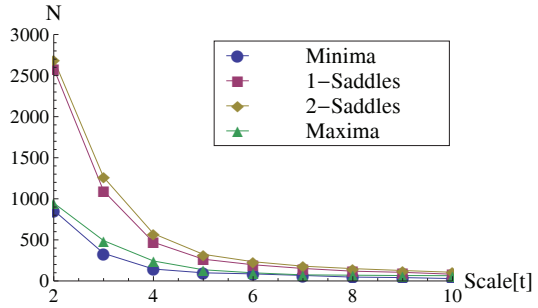


Fig. 1. Number of critical points versus scale, for frame 10; the scale is equal to $\sigma^2/2$, where σ is the width of the used Gaussian kernel.

3.2. Cardiovascular blood flow

We furthermore investigate saddle point extraction for time-resolved volumetric blood flow fields, acquired by PC-MRI. The velocity information is measured throughout the cardiac

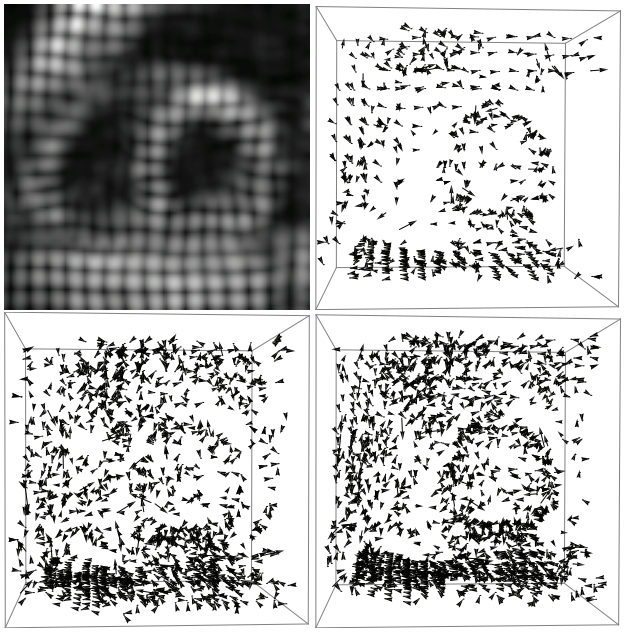


Fig. 2. Top left: Short axis view of tagged MR images, at frame 7; left ventricle on right-hand side of the image. Corresponding 3D velocity field of the cardiac muscle, based on tracking of maxima (top right), 1-saddles (bottom left), and 2-saddles (bottom right), at a scale of 3.

cycle, and is subsequently reconstructed at twenty phases in time, with a temporal resolution of approximately 40 ms. Every phase of the 4D flow data set entails a volumetric vector field, with a 3D velocity $\vec{v} = (v^1, v^2, v^3)$ at each voxel location. A typical data set comprises $150 \times 150 \times 50$ voxels, with a voxel size of $2 \times 2 \times 2.5$ mm^3. Fig. 3 gives an impression of the data.

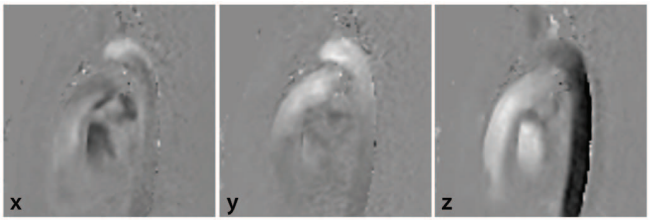


Fig. 3. A sagittal slice of one phase of 4D PC-MRI blood flow velocity data, depicted by the directions of acquisition at systole, where x conveys the flow in right-to-left direction, y in anterior-to-posterior direction and z in feet-to-head direction.

Before examining saddle points in a blood flow field, we need to understand the influence of noise on saddle point extraction. Gradient calculations are sensitive to noise, possibly jeopardizing the extraction results. The data is affected by conventional MRI acquisition noise, which follows a Rician distribution [22]. We employ the signal-to-noise ratio (SNR) as a quality measure, which in our case is determined by computing the ratio between the signal averages of a selected foreground region, containing high-speed flow, and a background region. For the measured velocity data, the unitless SNR values are typically better than 200. Experiments on artificial data confirm that saddle point extraction is robust to these levels of noise. We have generated a test data set given by $\vec{v} = (x, y, -z)$, containing a single 1-saddle at $\mathbf{x} = 0$. We superimpose varying levels of noise, which are linearly related to the mean of the vector magnitudes. For all experiments, covering a SNR range from 250 to 5, only 1-saddles where detected.

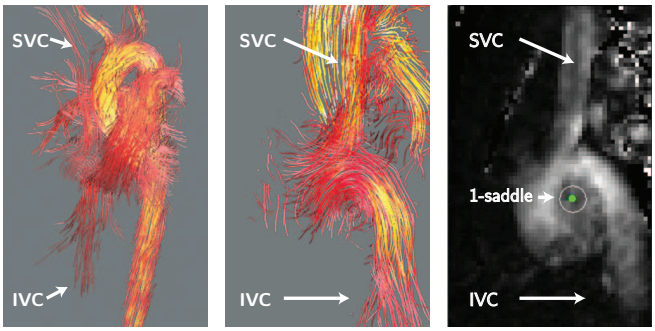


Fig. 4. (a)-(b) Pathlines convey the time-resolved volumetric blood flow in a volunteer study. Color codes the flow speed, with a lighter color representing a faster flow. (a) Cardiovascular system at peak systole. (b) We zoom in on the dynamics of the bloodstream into the right atrium. (c) A 1-saddle is detected within the right atrium, where the inflow streams meet.

The winding number algorithm is applied to the blood flow data set, at a fixed small scale comprising a neighborhood of $3 \times 3 \times 3$ voxels. The reason is that subtle flow variations are readily affected by the spatial resolution, and associated partial volume effects. A fixed small scale is therefore necessary to retain the necessary detail in the flow dynamics. We focus on the cardiac right atrium. Here, hemodynamics is characterized by a congregation of the inflow from the superior vena cava (SVC) and the inferior vena cava (IVC), in which case saddle points are expected. Extrema should not occur in the divergence-free blood flow fields (e.g., [12]). The algorithm detects a single 1-saddle within the right atrium, as depicted in Fig. 4(c). This point is detected over five phases of the cardiac cycle, roughly comprising the systolic time span of a heartbeat. The consistent detection in both space and time makes us confident that the found saddle point is not related to acquisition artifacts.

4. CONCLUSIONS

We have presented novel results on detection of 3D saddle points in cardiac imaging. We have examined the dependence on scale of detected critical points in 3D tagged MRI

images, and estimated cardiac motion by computing velocity fields based on different types of critical points. We preliminary conclude that velocity fields based on saddle points are preferable to those based on maxima, since they are more dense and therefore the vector field reconstructions are better supported by data evidence and less affected by extrinsic interpolation or regularization hypotheses. It is also clear from the results that a combined approach using maxima and both types of saddles further improves vector field reconstructions. However, the stability of detected saddle points through the image sequence should still be assessed.

We have also performed a feasibility study of critical point detection in measured flow data, obtaining promising results. Note that in the literature, critical point extraction is studied almost exclusively on analytical vector fields. Our method should be assessed further by experiments on more data sets, including pathological flow data. In the case of vector fields, critical points with complex Jacobian eigenvalues can occur. Although our method can potentially detect such points, this aspect should be developed further to achieve a confident detection. We have also observed that noise addition in analytical vector fields can change the character of a critical point from real to complex, in the Jacobian eigenvalues sense. In future work we will address this issue for measured flow data.

5. REFERENCES

[1] G. Wollny, M. Tittgemeyer, and F. Kruggel, "Segmentation of vector fields by critical point analysis: Application to brain deformation," in *Proceedings of International Conference on Pattern Recognition*, 2002, pp. 524–527.

[2] K. Habuka and Y. Shinagawa, "Image interpolation using enhanced multiresolution critical-point filters," *Int. J. Comput. Vision*, vol. 58, no. 1, pp. 19–35, 2004.

[3] B. Platel, E. Balmachnova, L. Florack, and B.M. ter Haar Romeny, "Top-points as interest points for image matching," in *ECCV (1)*. 2006, vol. 3951 of *Lecture Notes in Computer Science*, pp. 418–429, Springer.

[4] A. Becciu, H. C. van Assen, L. M. J Florack, S. Kozerke, V. J. Roode, and B. M. ter Haar Romeny, "A multi-scale feature based optic flow method for 3D cardiac motion estimation," in *SSVM '09*, 2009, vol. 5567, pp. 588–599.

[5] J. Blom, *Topological and geometrical aspects of image structure*, Ph.D. thesis, University of Utrecht, Department of Medical and Physiological Physics, 1992.

[6] R.N. Lee, "Two-dimensional critical point configuration graphs," *IEEE Trans. Pattern Anal. Mach. Intell.*, vol. 6, no. 4, pp. 442–450, 1984.

[7] A. Kuijper, "On detecting all saddle points in 2D images," *Pattern Recogn. Lett.*, vol. 25, pp. 1665–1672, November 2004.

[8] L. Pan, J. Prince, J. Lima, and N.F. Osman, "Fast tracking of cardiac motion using 3D-HARP," *IEEE transactions on Biomedical Engineering*, vol. 52, no. 8, pp. 1425–1435, 2005.

[9] T. Chen, X. Wang, S. Chung, D.N. Metaxas, and L. Axel, "Automated 3D motion tracking using gabor filter bank, robust point matching, and deformable models," *IEEE Trans. Med. Imaging*, vol. 29, no. 1, pp. 1–11, 2010.

[10] E. Oubel, M.D. Craene, A.O. Hero, A. Pourmorteza, M. Huguet, G. Avegliano, B. Bijnens, and A.F. Frangi, "Cardiac motion estimation by joint alignment of tagged MRI sequences," *Medical Image Analysis*, vol. 16, no. 1, pp. 339–350, 2012.

[11] R.S. Laramee, H. Hauser, L. Zhao, and F.H. Post, "Topology-based flow visualization, the state of the art," *Topology-based methods in visualization. Berlin: Springer*, pp. 1–19, 2007.

[12] H. Theisel, T. Weinkauf, H.C. Hege, and H.P. Seidel, "Saddle connectors – an approach to visualizing the topological skeleton of complex 3D vector fields," in *Proc. IEEE Visualization*, 2003, pp. 225–232.

[13] A. Becciu, A. Fuster, M. Pottek, B. van den Heuvel, B.M. ter Haar Romeny, and H. van Assen, "3D winding number: Theory and application to medical imaging," *International Journal of Biomedical Imaging*, vol. 2011, no. Article ID 516942, 2011.

[14] S.N. Kalitzin, B.M. ter Haar Romeny, A.H. Salden, P.F.M. Nacken, and M.A. Viergever, "Topological numbers and singularities in scalar images: Scale-space evolution properties," *Journal of Mathematical Imaging and Vision*, vol. 9, pp. 253–269, 1998.

[15] B.M. ter Haar Romeny, B. Titulaer, S.N. Kalitzin, G. Scheffer, F. Broekmans, J.J. Staal, and E. te Velde, "Computer assisted human follicle analysis for fertility prospects with 3D ultrasound," in *IPMI*, 1999, vol. 1613 of *Lecture Notes in Computer Science*, p. 5669.

[16] T. Lindeberg, *Scale-space theory in computer vision*, The Kluwer International Series in Engineering and Computer Science. Dordrecht, The Netherlands, 1994.

[17] L. M. J. Florack, *Image Structure*, Computational imaging and vision. Kluwer Academic Publishers, Dordrecht, The Netherlands, 1997.

[18] X. Tricoche, T. Wischgoll, G. Scheuermann, and H. Hagen, "Topology tracking for the visualization of time-dependent two-dimensional flows," *Computers and Graphics*, vol. 26, pp. 2002, 2002.

[19] S. Mann and A.P. Rockwood, "Computing singularities of 3D vector fields with geometric algebra," in *IEEE Visualization*, 2002, pp. 283–290.

[20] Klein, T. and Ertl, T., " Scale-Space Tracking of Critical Points in 3D Vector Fields ," in *Topology-Based Methods in Visualization*. 2007 , pp. 35–49 , Springer .

[21] A.K. Rutz, S. Ryf, S. Plein, P. Boesiger, and S. Kozerke, "Accelerated whole-heart 3D CSPAMM for myocardial motion quantification," *Magnetic Resonance in Medicine*, vol. 59, no. 4, pp. 755–763, 2008.

[22] H. Gudbjartsson and S. Patz, "The Rician distribution of noisy MRI data.," *Magnetic Resonance in Medicine*, vol. 34, no. 6, pp. 910–914, Dec. 1995.